A solid-state nuclear clock in an eccentric Earth orbit as a null test of local position invariance

New York General Group, Inc.

17 November 2026

Abstract

Einstein's equivalence principle requires that the ratio of two co-located frequency standards be independent of where they sit in a gravitational potential. The strongest bound on a gravitational coupling of the fine-structure constant α, $c^2\,\mathrm{d}\ln\alpha/\mathrm{d}\Phi = 14(11)\times10^{-9}$, rests on the annual modulation of the Sun's potential at Earth[1]. Here we propose THEO (Thorium Eccentric Orbiter), a satellite that compares the 148.4 nm nuclear transition of ^{229}Th in a fluoride crystal with the length of a single-crystal silicon resonator. One laser serves both references, with no frequency comb and no link to the ground. The nuclear transition is about 5,900 times more sensitive to α than the resonator[2]. A 12-hour orbit with 1,000 km perigee altitude modulates the potential by 5.0×10^{-10} peak to peak, at a period where laboratory solid-state nuclear clocks already show white frequency noise[3]. We derive a closed-form sensitivity law and show that the statistically optimal eccentricity at fixed perigee is e ≈ 0.58. With the already-demonstrated instability of $3\times10^{-12}\,\tau^{-1/2}$, about four orbits would equal the statistical precision of the present bound. Three years would reach $\delta k_\alpha \approx 5\times10^{-10}$, and projected clock improvements would reach 10^{-12}–10^{-13}. These figures are statistical, assume laboratory performance is reproduced in orbit, and scale as 5,900/K. The mission would also map α radially between 1.16 and 7.2 Earth radii.

Main

Local position invariance (LPI) states that the outcome of a local non-gravitational experiment does not depend on where or when it is performed[4]. Any light scalar field that couples to matter and is sourced by massive bodies would violate it, by making α, the electron mass or the quark masses depend on the local potential[5,6]. Experimentally, LPI is tested in two ways.

- **Absolute redshift tests** compare a clock in space with one on the ground. They include Gravity Probe A[7] and the eccentric Galileo satellites[8,9], which reached the 10^{-5} level. These need time and frequency transfer and precise orbit knowledge.
- **Null tests** compare two dissimilar clocks at one location as the potential changes. They need neither. Their reach is set by the difference in sensitivity of the two clocks to the constants. For electronic transitions the largest known sensitivity to α is K ≈ −6 (the Yb^+ octupole transition)[1,2].

The ^{229}Th nucleus changes this second factor by three orders of magnitude. Its 8.36 eV isomeric transition arises from a near-cancellation of Coulomb and strong-interaction energies[10,11]. It has been laser-excited in crystals[12,13] and measured at 2,020,407,384,335(2) kHz[14]. Its α-sensitivity is K = 5,900(2,300)[2]. Continuous-wave sources at 148.4 nm now exist[15,16]. A laser has been locked to the nuclear line in a room-temperature Th:CaF_2 crystal by continuous absorption spectroscopy, with instability $3\times10^{-12}(\tau/\mathrm{s})^{-1/2}$ averaging down to about 10^{-15} at one day[3,17]. A temperature of 196(5) K has been identified at which the first-order thermal sensitivity of one quadrupole line vanishes[18,19].

A solid-state nuclear clock has a weakness that matters here. Its transition frequency is reproducible between crystals and over months only at the 10^{-13} level[18]. A ground-based search for the annual solar modulation, at 3×10^{-8} Hz, would therefore be limited by slow drift and not by the white-noise instability. The proposal is to move the signal to a frequency where the clock is demonstrably white, by carrying it through Earth's own potential on an eccentric orbit.

Earlier concepts supply the ingredients:

- dual-clock eccentric-orbit missions with electronic references[20];
- a single optical clock in an eccentric orbit[21];
- nuclear clocks on an inner-Solar-System probe to search for dark matter bound to the Sun[22].

To our knowledge these have not been combined into an all-solid-state, comb-free nuclear–electronic null test in Earth orbit.

Measurement principle

Let $u(\mathbf{r}) \equiv GM/(rc^2)$ be the dimensionless Newtonian potential of Earth. For a frequency standard X, define sensitivities $A_X^{(j)} = \partial \ln \nu_X / \partial \ln g_j$ to the dimensionless constants $g_j \in \{\alpha,\ X_e = m_e/\Lambda_{\rm QCD},\ X_q = m_q/\Lambda_{\rm QCD}\}$. Define LPI coefficients $k_j \equiv \partial \ln g_j / \partial u$. For two co-located standards the universal gravitational redshift and the first- and second-order Doppler shifts are identical and cancel in the ratio. What remains is

$$y(t) \equiv \frac{\delta(\nu_{\rm Th}/\nu_{\rm cav})}{\nu_{\rm Th}/\nu_{\rm cav}} = \kappa\,[u(t) - \bar{u}], \qquad \kappa = \sum_j (A_{\rm Th}^{(j)} - A_{\rm cav}^{(j)}) k_j. \tag{1}$$

The equivalence principle predicts κ = 0.

A resonator of length L built from a crystal has $L \propto a_{\rm B} = \hbar/(m_e c\,\alpha)$, so $\nu_{\rm cav} \propto \alpha m_e$. This gives $A_{\rm cav}^{(\alpha)} = 1$ and $A_{\rm cav}^{(X_e)} = 1$ to leading order. The nuclear line has $A_{\rm Th}^{(\alpha)} = K$ and a quark-mass sensitivity K_q that is expected to be large but is poorly known[10]. Hence

$$\kappa = (K-1)\,k_\alpha - k_e + K_q\,k_q. \tag{2}$$

The experiment measures κ. Quoting a bound on k_α alone assumes the other terms do not cancel it, and inherits the 40% uncertainty of K.

The orbit as a modulator

On a Kepler orbit with semi-major axis a, eccentricity e and mean anomaly M,

$$\frac{a}{r} = 1 + 2\sum_{k\geq 1} J_k(ke)\cos kM, \tag{3}$$

so the signal is a comb of harmonics of the orbital frequency with amplitudes fixed by Bessel functions:

$$y(t) = \kappa\,\frac{2GM}{ac^2}\sum_{k\geq 1} J_k(ke)\cos kM(t). \tag{4}$$

The signal is even about perigee and instantaneous, and it has no free shape parameter. Using the time averages $\langle a/r\rangle = 1$ and $\langle a^2/r^2\rangle = (1-e^2)^{-1/2}$, the r.m.s. modulation is

$$\sigma_u = \frac{GM}{ac^2}\Big[(1-e^2)^{-1/2} - 1\Big]^{1/2}. \tag{5}$$

Optimal eccentricity. For fixed perigee radius $r_p = a(1-e)$, equation (5) becomes $\sigma_u = \frac{GM}{r_p c^2}\,(1-e)\,[(1-e^2)^{-1/2} - 1]^{1/2}$. The modulation vanishes for e → 0. It also vanishes for e → 1, because the satellite then spends almost all its time near apogee. The maximum satisfies

$$2(1-e^2)\big[1-\sqrt{1-e^2}\big] = e(1-e) \;\Rightarrow\; e^* \approx 0.58, \qquad \sigma_u^{\rm max} \approx 0.200\,\frac{GM}{r_p c^2}. \tag{6}$$

The optimum is flat. We adopt the 12-hour, critically inclined orbit of Table 1 instead. It gives up 7% of σ_u in exchange for a repeating ground track, a frozen perigee latitude and an apogee beyond the heart of the outer radiation belt.

Table 1 | Baseline orbit and potential modulation (calculated)

Quantity	Value
Perigee altitude / radius	1,000 km / 7,378 km
Semi-major axis, eccentricity	26,562 km, 0.7222
Apogee altitude	39,368 km
Period	43,083 s (11.97 h)
Inclination	63.4° (apsidal line frozen); nodal regression ≈ −0.13° per day
$GM/(ac^2)$	1.670×10^{-10}
Peak-to-peak Δu	5.04×10^{-10}
r.m.s. σ_u (eq. 5)	1.115×10^{-10}
Harmonic amplitudes $2\frac{GM}{ac^2} J_k(ke)$, k = 1, 2, 3	$1.13,\ 0.73,\ 0.52\ (\times 10^{-10})$
Signal power in k ≤ 3	84% (51% in the fundamental)
Fraction of time with r < 15,000 km	11%
Common-mode relativistic modulation of each reference	$\approx 1 \times 10^{-9}$ peak to peak (cancels in the ratio)

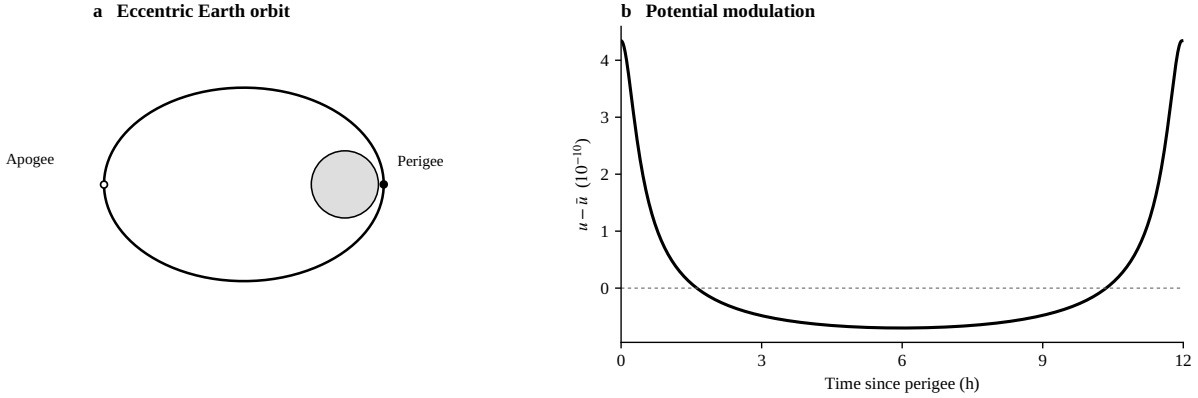


Fig. 2 | Orbit geometry and potential modulation. Calculated from the baseline orbit in Table 1 and equations (3)–(5).

The solar annual modulation used on the ground has r.m.s. 1.17×10^{-10}, essentially the same as σ_u here. The orbit therefore does not buy statistical leverage per unit time over an ideal, drift-free ground experiment. It buys three other things:

1. a signal at 2.3×10^{-5} Hz and its harmonics, where white noise has been demonstrated, instead of 3×10^{-8} Hz, where it has not;
2. Earth instead of the Sun as the source body;
3. a 6.2-fold range in distance from the source on every orbit.

Payload architecture

The payload has three solid elements and no atoms in the gas phase (Fig. 1).

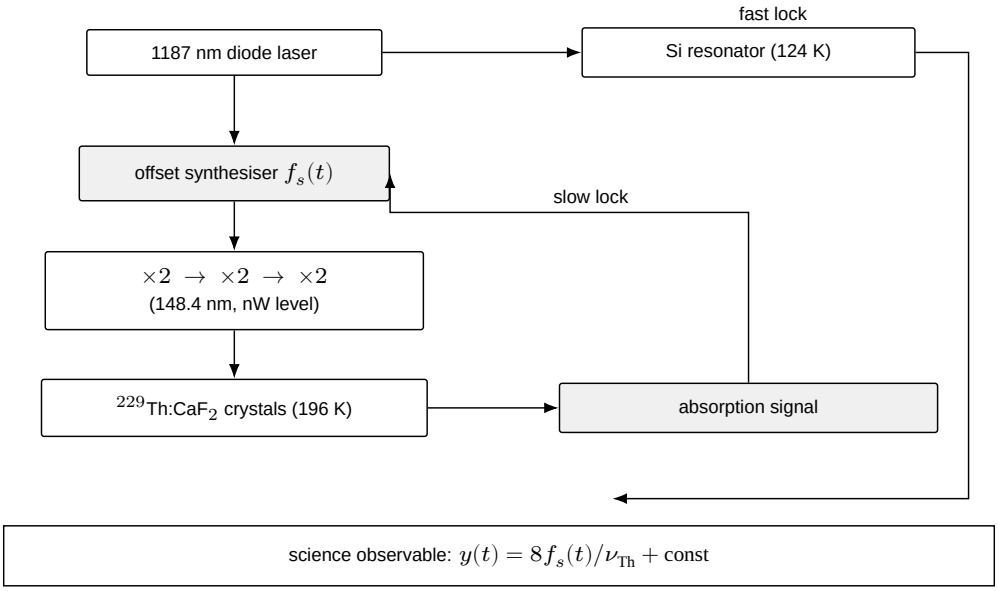


Fig. 1 | Signal chain. The correction that keeps the eighth harmonic on the nuclear line is itself the measurement.

- **Laser and conversion.** A 1,187 nm diode laser is frequency-doubled three times to 148.4 nm, the route demonstrated in the laboratory at nanowatt power[15].
- **Electronic reference.** The laser is locked on short timescales to a single-crystal silicon resonator held at its thermal-expansion zero near 124 K[23].
- **Nuclear reference.** A radio-frequency offset $f_s(t)$ steers the eighth harmonic onto the nuclear line, which is detected in absorption[17]. The record of f_s is the ratio $\nu_{\mathrm{Th}}/8\nu_{\mathrm{cav}}$. A radio-frequency reference accurate to 10^{-11} is sufficient.
- **Two operating temperatures.** The crystal is held at 196 K (ref. 18) and the resonator at 124 K (ref. 23). Blackbody emittances at these temperatures are 84 and 13 W m^{-2}. Shaded radiators of a few tenths of a square metre therefore reject watt-level loads, and we expect both set-points to be reachable passively over most of this orbit. This expectation has not been verified by a thermal model.
- **Built-in diagnostics.** Other quadrupole-split lines of the same crystal have non-zero temperature slopes and serve as in-situ thermometers[18]. Two crystals with different dopant concentrations, or different hosts, share the nuclear signal but not the host-dependent shifts.

Projected sensitivity

For white frequency noise with $\sigma_y(\tau) = \sigma_1 \tau^{-1/2}$, the least-squares estimate of κ from a record of duration T has variance (Methods)

$$\delta\kappa = \frac{\sigma_1}{\sigma_u \sqrt{T}}, \qquad \delta k_\alpha = \frac{\sigma_1}{(K-1)\,\dfrac{GM}{ac^2}\sqrt{T\left[(1-e^2)^{-1/2}-1\right]}}. \tag{7}$$

Table 2 | Statistical reach for three years at 80% duty (T = 7.57 × 10⁷ s), K = 5,900

Scenario	σ_1 (s$^{1/2}$)	$\delta\kappa$	δk_α	Gain over ref. 1 (1.1 × 10^{-8})
A: laboratory instability already demonstrated[3]	3×10^{-12}	3.1×10^{-6}	5.2×10^{-10}	≈ 21
B: projected	1×10^{-14}	1.0×10^{-8}	1.7×10^{-12}	≈ 6 × 10^3
C: projected	1×10^{-15}	1.0×10^{-9}	1.7×10^{-13}	≈ 6 × 10^4

Three points qualify these numbers.

- **Scenario A is fast.** A single orbit gives $\delta k_\alpha = 2.2 \times 10^{-8}$, so about four orbits (two days) match the present

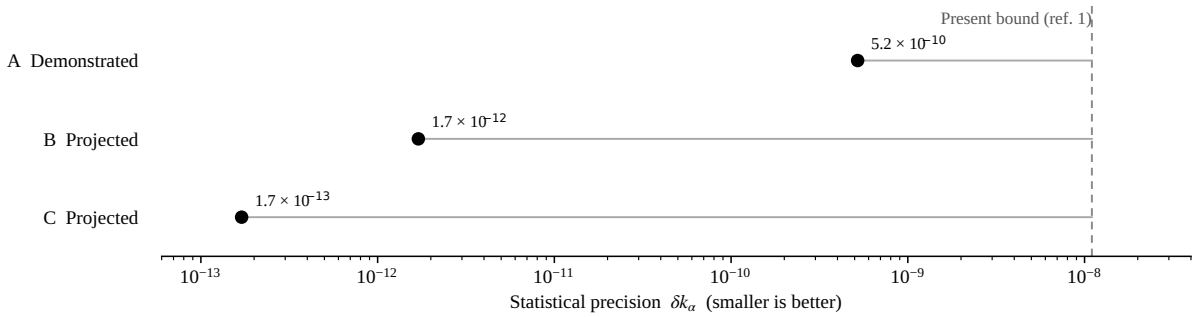


Fig. 3 | Statistical reach. Three-year precision at 80% duty for the scenarios in Table 2, compared with the present bound.

bound statistically.

- **Scenarios B and C are projections.** They rest on the expectation, stated in ref. 3 but not yet demonstrated, that solid-state nuclear clocks can improve by several orders of magnitude.
- **All rows depend on K.** They scale as 5,900/K, so the ±2,300 uncertainty of K moves each entry by a factor of between 0.7 and 1.6.

Radial tomography of α and finite-range fields

The orbit samples radius with dwell-time density

$$p(r) = \frac{r}{\pi a \sqrt{a^2 e^2 - (r-a)^2}}, \qquad a(1-e) \le r \le a(1+e), \tag{8}$$

so the ratio can be averaged in radial bins without assuming a 1/r law. A bin holding a fraction p_j of the time is resolved to $\sigma_1/\sqrt{T p_j}$. In scenario A, the mean of α below 15,000 km would be compared with its mean over the rest of the orbit to a statistical precision of about 2×10^{-19}.

This matters for fields of finite range λ. A scalar of mass $m_\phi = \hbar/(\lambda c)$, sourced by a uniform sphere of radius R, replaces the template by

$$u_\lambda(r) = \frac{GM}{rc^2}\,\Phi\!\left(\frac{R}{\lambda}\right) e^{-r/\lambda}, \qquad \Phi(x) = \frac{3(x\cosh x - \sinh x)}{x^3}. \tag{9}$$

For λ between about 2 × 10³ and 10⁵ km ($m_\phi c^2 \approx 10^{-13}$ to 2×10^{-15} eV) the exponential changes appreciably between perigee and apogee, so the shape of the profile carries information on λ. A solar-modulation experiment on the ground has almost no sensitivity to such fields. For scalars coupled quadratically, the field amplitude near Earth acquires a 1/r-dependent static profile[24]. This is the same observable, with a different interpretation of κ.

Systematic effects locked to the orbit

Only perturbations that repeat with the orbit and have a component along the template (4) bias κ. Table 3 lists those we have identified.

Table 3 | Orbit-synchronous effects (estimates; see Methods)

Effect	Radial law	Unmitigated size	Mitigation	Requirement
Universal redshift and Doppler	r^{-1}	10^{-9} per reference	Cancels identically in the ratio	Orbit known to ~1 km for the template
Geomagnetic Zeeman shift of the nuclear line	r^{-3}, vector	~10² Hz per ±m component (~10⁻¹³), opposite signs	Symmetric probing of ±m; magnetic shield	Shield factor ≥ 10³ and polarisation asymmetry ≤ 10⁻² give ≤ 10⁻¹⁸
Tidal elastic strain of the resonator	r^{-3}, tensor	2 × 10⁻¹⁷ at perigee (10 cm Si)	Deterministic; calibrate by attitude slews	Calibration to 1%

Effect	Radial law	Unmitigated size	Mitigation	Requirement
Earth infrared and albedo heating	$\approx r^{-2}$, low-pass filtered	Design-dependent	Multi-stage passive filtering; nuclear-line thermometry as regressor	Synchronous δT ≤ 1 mK (crystal), ≤ 1 μK (resonator)
Trapped-radiation dose rate	Peaks at belt crossings, not at perigee	Not yet modelled	Shielding; gated detection; dose-rate monitor as regressor	Transport analysis needed
Solar eclipse transients	Tied to Sun direction	Design-dependent	Phase drifts through the year relative to perigee	—

Four discriminators separate a real signal from these.

1. **Harmonic fingerprint.** The ratios $J_2(2e)/J_1(e) = 0.646$ and $J_3(3e)/J_1(e) = 0.463$ are fixed. Effects scaling as r^{-2} or r^{-3}, or filtered by a thermal time constant, have different ratios and phases.
2. **Attitude slews.** These change the thermal, magnetic and tidal couplings but not u.
3. **Solar geometry.** The Sun direction rotates through 360° per year relative to the apsidal line, while the LPI signal does not.
4. **Perigee change.** Raising the perigee mid-mission changes the signal by a factor known in advance from equation (5).

Discussion

What a result would mean. A null result at the level of Table 2 would tighten the bound on a gravitational coupling of α by between one and almost five orders of magnitude, and would do so for a terrestrial source instead of a solar one. A non-zero κ that showed the harmonic ratios of equation (4), survived attitude slews and rescaled correctly after a perigee change would be evidence for a violation of the equivalence principle.

Relation to free-fall tests. For the simplest linearly coupled dilaton models, free-fall experiments such as MICROSCOPE[25] (Eötvös parameter bounded at the 10^{-15} level) probably remain more constraining over much of the parameter space[5]. Clock tests measure a different combination of couplings. They are independent of assumptions about how the field couples to bulk matter, and they give a direct radial profile.

What is not established. We consider the physics of the measurement secure. The following are not:

- operation of a 148 nm source and its optics for years in orbit;
- the behaviour of Th:CaF_2 under trapped-radiation dose, including transmission loss and radioluminescence;
- the curvature of the frequency–temperature relation at 196 K, which sets the thermal requirement (we assumed 10^{-15}–10^{-14} K^{-2} as an order of magnitude);
- resonator stability at 12 hours in flight;
- mass, power and station-keeping budgets, which we have not derived.

Order of work. The logical order of risk retirement is:

1. a laboratory demonstration of the comb-free resonator-referenced ratio with white noise out to 12 hours;
2. irradiation of doped crystals to the mission dose;
3. a low-orbit pathfinder for the VUV chain.

Only the first exists in part today[3].

Methods

Kepler averages. With eccentric anomaly E, $r = a(1-e\cos E)$ and $\mathrm{d}M = (r/a)\,\mathrm{d}E$. Then $\langle a/r\rangle = \frac{1}{2\pi}\oint \mathrm{d}E = 1$ and $\langle a^2/r^2\rangle = \frac{1}{2\pi}\oint \frac{\mathrm{d}E}{1-e\cos E} = (1-e^2)^{-1/2}$, which gives equation (5). Parseval's relation applied to equation (3) gives $2\sum_k J_k^2(ke) = (1-e^2)^{-1/2} - 1 = 0.4458$ for the baseline. The first three terms contribute 0.3729.

Estimator. Model $y(t) = \kappa\tilde{u}(t) + n(t)$ with $\tilde{u} = u - \langle u\rangle$ and one-sided noise density $S_y = 2\sigma_1^2$. The minimum-variance linear estimator is $\hat{\kappa} = \int y\tilde{u}\,\mathrm{d}t / \int \tilde{u}^2\mathrm{d}t$, with $\mathrm{Var}\,\hat{\kappa} = (S_y/2)/\int \tilde{u}^2\mathrm{d}t = \sigma_1^2/(T\sigma_u^2)$. Analysing apogee-

to-apogee segments makes $\tilde{u}$ even about the segment centre, so a constant offset and a linear drift per segment are orthogonal to it and cost no sensitivity. If a measured regressor (temperature or dose rate) with correlation coefficient ρ to $\tilde{u}$ is fitted jointly, the variance is inflated by $1/(1-\rho^2)$.

Dwell density. From $\dot{r}^2 = \frac{\mu}{ar^2}\,[a^2e^2-(r-a)^2]$ and $p(r) = 2/(P|\dot{r}|)$, equation (8) follows. The substitution $r - a = ae\sin\theta$ verifies its normalisation.

Optimal eccentricity. Setting $\mathrm{d}/\mathrm{d}e$ of $(1-e)^2[(1-e^2)^{-1/2}-1]$ to zero gives equation (6). Numerically the maximum is 0.04015 at e ≈ 0.576, against 0.03440 at e = 0.7222, a ratio of 0.926 in σ_u.

Tidal strain. In a non-rotating frame the tidal body force per unit volume on the spacer is $\rho\,(\mu/r^3)(3\hat{r}\hat{r}-\mathbb{1})\cdot\mathbf{x}$. For a free rod of length L, density ρ and Young's modulus Y, with axis at angle θ to $\hat{r}$, the leading axial elongation is

$$\frac{\delta L}{L} = \frac{\rho L^2}{12Y}\,\frac{\mu}{r^3}\,(3\cos^2\theta - 1).$$

With ρ = 2,330 kg m^{-3}, L = 0.1 m, Y = 1.9 × 10^{11} Pa and $\mu/r_p^3 = 9.9\times10^{-7}$ s^{-2}, this is 2 × 10^{-17} at θ = 0. The term vanishes at $\cos^2\theta = 1/3$. Transverse and rotational terms are not included.

Zeeman estimate. The dipole field at perigee is 20–40 μT. With nuclear moments of a few tenths of a nuclear magneton ($\mu_N/h = 7.62$ MHz T^{-1}), individual ±m components shift by order 10² Hz with opposite signs. The centroid is unshifted to first order. The second-order shift, of order (10² Hz)² divided by the ~10⁸ Hz quadrupole splitting, is below 10^{-19} fractionally.

Thermal filtering. A passive stage of time constant τ_{th} attenuates the k-th harmonic by $[1+(kn\tau_{\mathrm{th}})^2]^{-1/2}$, with $n = 1.458\times10^{-4}$ rad s^{-1}. This is 0.068 for the fundamental at $\tau_{\mathrm{th}} = 10^5$ s. Near the turning point T_0, the crystal shift is $\frac{1}{2}c_2(T-T_0)^2$. A set-point error ΔT_0 and a synchronous excursion δT give a fractional shift $c_2\,\Delta T_0\,\delta T$.

Data availability. No data were generated. All numbers follow from the equations and constants stated.

References

1. Lange, R. et al. Improved limits for violations of local position invariance from atomic clock comparisons. *Phys. Rev. Lett.* **126**, 011102 (2021).
2. Beeks, K. et al. Fine-structure constant sensitivity of the Th-229 nuclear clock transition. *Nat. Commun.* (2025). doi:10.1038/s41467-025-64191-7.
3. A thorium-229 optical nuclear clock with feedback loop. Preprint, arXiv:2606.04997 (2026).
4. Will, C. M. The confrontation between general relativity and experiment. *Living Rev. Relativ.* **17**, 4 (2014).
5. Damour, T. & Donoghue, J. F. Equivalence principle violations and couplings of a light dilaton. *Phys. Rev. D* **82**, 084033 (2010).
6. Uzan, J.-P. Varying constants, gravitation and cosmology. *Living Rev. Relativ.* **14**, 2 (2011).
7. Vessot, R. F. C. et al. Test of relativistic gravitation with a space-borne hydrogen maser. *Phys. Rev. Lett.* **45**, 2081–2084 (1980).
8. Delva, P. et al. Gravitational redshift test using eccentric Galileo satellites. *Phys. Rev. Lett.* **121**, 231101 (2018).
9. Herrmann, S. et al. Test of the gravitational redshift with Galileo satellites in an eccentric orbit. *Phys. Rev. Lett.* **121**, 231102 (2018).
10. Flambaum, V. V. Enhanced effect of temporal variation of the fine structure constant and the strong interaction in ^{229}Th. *Phys. Rev. Lett.* **97**, 092502 (2006).
11. Peik, E. & Tamm, C. Nuclear laser spectroscopy of the 3.5 eV transition in Th-229. *Europhys. Lett.* **61**, 181–186 (2003).
12. Tiedau, J. et al. Laser excitation of the Th-229 nucleus. *Phys. Rev. Lett.* **132**, 182501 (2024).
13. Elwell, R. et al. Laser excitation of the ^{229}Th nuclear isomeric transition in a solid-state host. *Phys. Rev. Lett.* **133**, 013201 (2024).
14. Zhang, C. et al. Frequency ratio of the ^{229m}Th nuclear isomeric transition and the ^{87}Sr atomic clock. *Nature* **633**, 63–70 (2024).
15. Lal, V. et al. Continuous-wave laser source at the 148 nm nuclear transition of Th-229. *Optica* **12**, 1971 (2025).
16. A continuous-wave vacuum ultraviolet laser for the nuclear clock. Preprint, arXiv:2507.19449 (2025).
17. Continuous-wave laser absorption spectroscopy of the thorium-229 nucleus. Preprint, arXiv:2604.16640 (2026).

18. Ooi, T. et al. Frequency reproducibility of solid-state thorium-229 nuclear clocks. *Nature* (2026). doi:10.1038/s41586-025-09999-5.
19. Higgins, J. S. et al. Temperature sensitivity of a thorium-229 solid-state nuclear clock. *Phys. Rev. Lett.* **134**, 113801 (2025).
20. Schiller, S. et al. Einstein Gravity Explorer – a medium-class fundamental physics mission. *Exp. Astron.* **23**, 573–610 (2009).
21. Derevianko, A. et al. Fundamental physics with a state-of-the-art optical clock in space. *Quantum Sci. Technol.* **7**, 044002 (2022).
22. Tsai, Y.-D., Eby, J. & Safronova, M. S. Direct detection of ultralight dark matter bound to the Sun with space quantum sensors. *Nat. Astron.* **7**, 113–121 (2023).
23. Kessler, T. et al. A sub-40-mHz-linewidth laser based on a silicon single-crystal optical cavity. *Nat. Photon.* **6**, 687–692 (2012).
24. Hees, A., Minazzoli, O., Savalle, E., Stadnik, Y. V. & Wolf, P. Violation of the equivalence principle from light scalar dark matter. *Phys. Rev. D* **98**, 064051 (2018).
25. Touboul, P. et al. MICROSCOPE mission: final results of the test of the equivalence principle. *Phys. Rev. Lett.* **129**, 121102 (2022).